1 *Article*

2 # Non-destructive System Based on Electrical Tomography and Machine Learning to Analyze Moisture of Buildings

5 **Tomasz Rymarczyk[1] , Grzegorz Kłosowski[2], Edward Kozłowski[3]**

6 [1] University of Economics and Innovation in Lublin, Research & Development Centre Netrix S.A., Lublin,
7   Poland; tomasz@rymarczyk.com
8 [2] Faculty of Management, Lublin University of Technology, Lublin, Poland; g.klosowski@pollub.pl
9 [3] Faculty of Management, Lublin University of Technology, Lublin, Poland; e.kozlovski@pollub.pl

10
11

12 **Abstract:** The article presents the results of research on a new method of spatial analysis of walls
13 and buildings moisture. Due to the fact that destructive methods are not suitable for historical
14 buildings of great architectural significance, a non-destructive method based on electrical
15 tomography has been adopted. A hybrid tomograph with special sensors was developed for the
16 measurements. This device enables the acquisition of data, which are then reconstructed by
17 appropriately developed methods enabling spatial analysis of wet buildings. Special electrodes that
18 ensure good contact with the surface of porous building materials such as bricks and cement were
19 introduced. During the research, a group of algorithms enabling supervised machine learning was
20 analyzed. They have been used in the process of converting input electrical values into conductance
21 depicted by the output image pixels. The conductance values of individual pixels of the output
22 vector made it possible to obtain images of the interior of building walls, both flat intersections (2D)
23 and spatial (3D) images. The presented group of algorithms has a high application value. The main
24 advantages of the new methods are: high accuracy of imaging, low costs, high processing speed,
25 ease of application to walls of various thickness and irregular surface. By comparing the results of
26 tomographic reconstructions, the most efficient algorithms were identified.

27 **Keywords:** inverse problem; electrical tomography; moisture inspection; dampness analysis;
28 machine learning, nondestructive evaluation

29

1. Introduction

31   This article presents the results of research on the development of an effective and non-invasive
32 method for the detection of moisture walls and historical buildings. Humidity is one of the basic, and
33 at the same time undesirable, physical characteristics of building materials [1]. Detection of water
34 inside the walls of buildings and structures made of bricks or lightweight concrete and brick blocks
35 is one of the most frequently performed tests.

36   All buildings are exposed to various factors that erode the material which they are made. Such
37 factors include water [2]. Many buildings have damp walls and foundations [3]. This is evidenced by
38 often appearing molds and fungi, dark spots, detachment of plasters or paint coatings. This is
39 especially factual for older buildings. One of many reasons for this is the technology and materials
40 that were formerly used in construction, for example, lack of insulation. Moisture in the walls
41 significantly reduces their durability. The bricks and mortar that contain water are significantly
42 weakened and are less resistant to compression, which is particularly true for lime mortar. This
43 results in both deteriorations of the building's operational conditions and safety. In addition, the
44 water accumulated in the walls significantly worsens the thermal insulation properties of the walls

45 and contributes to the gradual erosion. Another important problem related to moisture in walls is
46 their harmful impact on inhabitant's health. Microclimate, which arises in rooms and walls with high
47 humidity often causes the formation of mold fungi that can cause respiratory diseases and
48 intoxication.
49   It can be argued that the main factor causing the destruction of the walls is just moisture. In
50 combination with daily temperature changes, moisture has the greatest impact on the overall strength
51 and durability of building structures. The water in the outer wall has a negative effect on the walls
52 regardless of the state of aggregation, i.e. in solid form (ice, snow), as a liquid (rain) and gas (water
53 vapor). Most structural defects, e.g. brick movements, cracking, molds, fungi, chemical reaction, are
54 initiated and compounded by the presence of moisture.
55   In order to reduce the risks associated with excessive humidity, moisture evaluations are
56 necessary for buildings [4]. Such tests can be helpful in determining the impact of rainwater and
57 groundwater, leakage and moisture from water supply and sewage systems as well as condensation
58 of water vapor.
59   Permeation of moisture in the walls of old buildings that are in direct contact with the soil, due
60 to the lack of a horizontal or vertical barrier separating the walls from water in the soil, leads to
61 migration of moisture (Figure 1). This leads to the migration of dissolved in water salt, which is
62 responsible for many construction problems. Building materials, both natural and man-made (e.g.,
63 the brick or concrete) are porous. Moisture from bricks and masonries can be drawn by gravity using
64 the capillary effect [5].
65   The condition of effective prevention of moisture in the building walls is its proper identification.
66 There are many methods that can generally be divided into two groups - destructive and non-
67 destructive methods. For obvious reasons, non-destructive methods are more desirable and have
68 bigger applied value [6, 7]. This feature is gaining importance when walls' humidity needs to be
69 measured in buildings of historical importance. Among the destructive methods can be
70 distinguished, among others, the "drying-weight" or "carbide" method. Unfortunately, this is an
71 invasive examination. The destructive methods consist in taking samples of the material being
72 examined, which is not always possible, especially in the case of historic buildings. In such cases,
73 these types of methods are not recommended, because they involve a violation of the structure of the
74 examined object. Therefore, non-invasive tests may be a better solution in such situations.
75   Non-destructive methods include, for example, thermovision or ultrasound methods. The
76 disadvantage of thermovision is its exterior, the impossibility of penetrating under the surface of the
77 investigated structure. The ultrasound approach is of little use due to the high porosity of materials
78 containing cells (pores) filled with air or water.
79   Non-destructive methods also include electrical impedance tomography (EIT), in which
80 electrical measurements are made [8]. This method, thanks to the measuring device and the
81 implemented algorithms, allows for non-invasive spatial determination of the degree of moisture. In
82 the case of impedance tomography, it is a technique for imaging the spatial distribution of
83 conductivity [9].
84   Previous studies show that electrical resistance can be used to measure the humidity of concrete
85 and masonry walls [10, 11, 12]. There is a known relationship between moisture inside a porous
86 building material and its electrical resistivity (Figure 2). Similar relationships can be observed for a
87 brick wall and a lightweight concrete blocks wall. The electrical resistance increases as the moisture
88 content decreases. It can be seen that the smallest change in resistance occurs in the highest range of
89 moisture content. Although current techniques for measuring moisture in concrete and brick walls
90 are accurate, the use of electrical resistance has the advantage of being a relatively simple procedure
91 that can be used with inexpensive equipment [13].
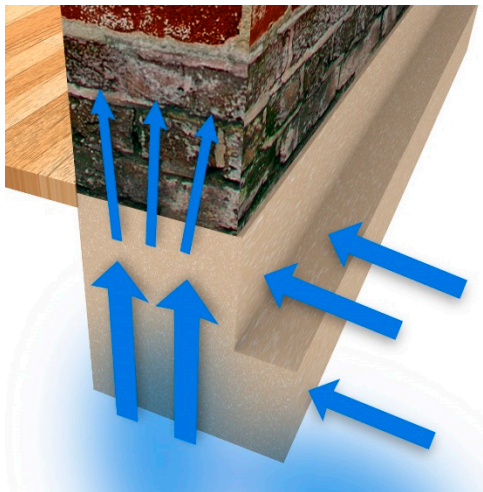
Figure 1. The rising moisture resulting from the direct connection of soil with masonry [14].
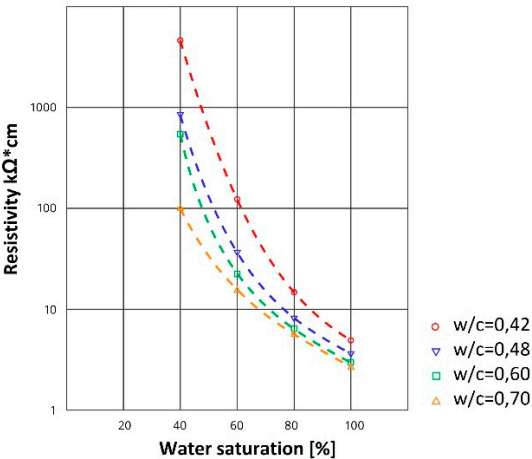
Figure 2. Relationship between saturation and resistivity of concrete [15].

92   Each measuring technique has its own conditions, advantages, and disadvantages. Thanks to
93   this it can be used only in special circumstances. Currently, the main problem in research on the
94   concentration of moisture in the walls is the lack of a method that provides spatial imaging of its
95   distribution inside the wall without the need to take samples. Most of the available research methods
96   allow only a spot evaluation of moisture, which makes it possible to obtain only a discrete model [4].
97   In most cases, methods based on real data are invasive.
98   This fact is a basic problem with regard to the analysis of thick walls because the moisture inside
99   each wall is usually a few percent higher than at its surface [16]. The destructive nature of currently
100 used techniques requiring sample collection is unacceptable, especially in historical buildings. In such
101 cases, only non-invasive methods may be used.
102 The humidity of the walls can be directly measured with electric meters. Electrical moisture
103 meters, in particular, conductivity meters, are, however, sensitive to very low amounts of moisture
104 and/or some types of contaminants with soluble salt. For example, a free moisture content lower than
105 0.1% can cause high meter readings. Due to the influence of salinity causing a change in electrical
106 resistance and a small depth of measurement, evaluations made with the use of electric humidity
107 meters should be considered as not very accurate [5, 16]. They can give an approximate image of the
108 dampness inside the walls (Figure 3).

109
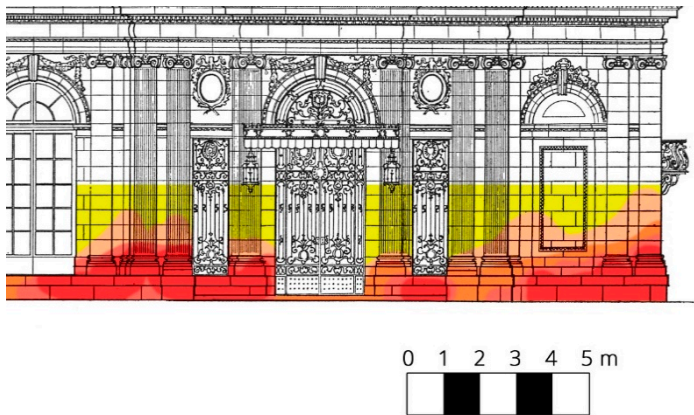
110 **Figure 3.** An image of building walls' dampness developed on the basis of the results of an electrical
111 test. Higher moisture concentrations are depicted by a color of higher intensity [17].

112   The main purpose of this study is to present and compare non-destructive algorithms based on
113   electrical tomography, which allow estimation of humidity not only on the wall surface but also
114   inside the masonry wall.
115   With reference to the tomography of building walls, the most commonly used methods are
116   impedance tomography (EIT), capacitance tomography (ECT) and resistive tomography (ERT). All
117   the above methods belong to the group of electrical tomography methods, including many
118   tomographic techniques showing the distribution of electrical parameters in the tested object [18, 19,
119   20] while the EIT shows the spatial distribution of conductivity γ [21, 22]. Authors such as Holder or
120   Karhunen et al. [23, 24] in the monograph give the general principles of the EIT, its instruments,
121   procedures, and challenges.
122   The proposed tomographic method in which the building materials humidity evaluation is an
123   indirect assessment based on a different physical characteristic, such as resistivity, allows for many
124   measurements (tomographic approach in [25, 26]) without the need to damage the tested object.
125   The tomographic approach allows archiving the moisture distribution inside the wall in a digital
126   form and comparing it with the next results in the future (moisture monitoring) when it is necessary.
127   This action is extremely useful in buildings requiring the use of a high imaging efficiency method, in
128   particular: constant monitoring of wall humidity, control of the effectiveness of the methods used for
129   drying walls and assessment of the moisture condition of load-bearing walls, in particular, thick ones.
130   The main advantages of the proposed measurement system are the non-invasive and non-
131   destructive measurement of the tested object thanks to specially designed electrodes (Figure 5), the
132   possibility of imaging the moisture distribution not only on the surface but also inside the
133   investigated object. The described research uses simulation tools based on the Matlab scientific
134   software and scripts in the Python and R programming languages. A special role was played by the
135   toolbox called EIDORS dedicated to the Matlab software [18]. It has been used for modeling domain
136   and topological algorithms using the finite element method (FEM) to solve the inverse problem (IP).
137   The structure of the article was divided into 5 parts including the introduction. Chapter 2
138   presents the hardware of the measurement system and algorithms for solving forward and inverse
139   problems. Section 3 presents the results of tests both in relation to simulation experiments and to the
140   reconstruction of the real object. The analysis covered 3 types of algorithms applicable in EIT: LARS,
141   ElasticNET and ANN. The real object was also reconstructed. Chapter 4 includes the comparison of
142   three selected algorithms and discussions in the perspective of previous studies. It also refers to other,
143   known methods within the studied issues. The possible improvements were suggested, too. Finally,
144   section 5 summarizes this article.

2. Materials and Methods

146   This chapter presents a measurement system that enabled the collection of electrical data used
147   subsequently to solve forward and inverse problems. Then there are short descriptions of four
148   selected algorithms: Least Angle Regression (LARS), ElasticNet, Artificial Neural Networks (ANN)
149   and Gauss-Newton. The first three methods were used in the experiments on tomographic imaging
150   and compared with each other. All tested algorithms are classified as machine learning and artificial
151   intelligence methods. Thanks to the above algorithms, it was possible to use the supervised machine
152   learning method, which in combination with the parallel computing (multi-core CPU, GPU) allowed
153   to quickly reach effective solutions in the field of building models of reconstructed objects.

2.1 Selected hardware issues, sample models and reconstructions

155   Electrical tomography is a technique for imaging the distribution of conductivity or permeability
156   inside an object under investigation based on measurements of the potential distribution on the
157   object's surface. Numerous different techniques can be used in the process of optimization of
158   tomographic methods.
159   The data collection system collects the measured voltage from the electrodes and then processes
160   the data. Conventional data acquisition systems require voltage, filtering, demodulation and
161   converting equipment to be digitized and a signal processor to transfer data to a computer. Our

162   device for measurement in electrical tomography uses two methods: electrical capacitance
163   tomography and electrical impedance tomography. It allows you to take measurements up to 32
164   channels. Figure 4 (a) shows the inside of the tomograph, while Figure 4 (b) shows the main panel of
165   the device with sockets designed to connect the electrodes. This device provides a non-invasive way
166   to test the spatial distribution of moisture. The system includes an additional software solutions. The
167   advantage of the system is the simultaneous measurement of voltage and capacitance.
168
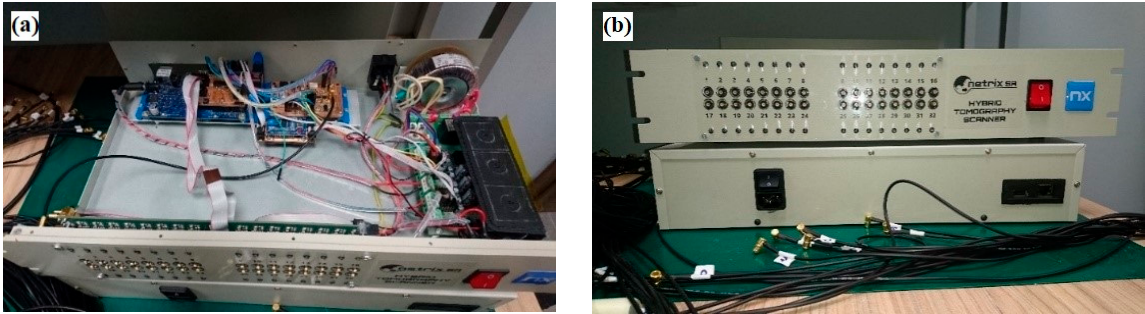
169   **Figure 4.** The measurement device

170   The measurements were made using the Polar GND EIT method, at 1 kHz frequency and 100uA
171   excitation current. An object whose internal electrical properties are unknown is surrounded by
172   electrodes placed on its edge and electrically excited in various combinations (see Figure 5).
173   Measurements are made for all possible ways of connecting the power source to the next pairs of
174   electrodes. Other electrodes measure voltage drops. Both parts of Figure 5 (a) and (b) shows two
175   exemplary measuring cycles. In this way a series of measurements is created. For a system with 16
176   electrodes (we mark them as variable *n*), there are 16 possibilities to connect the power source, but
177   because of the symmetry of the system, we accept only half of them ($n / 2 = 8$).

178
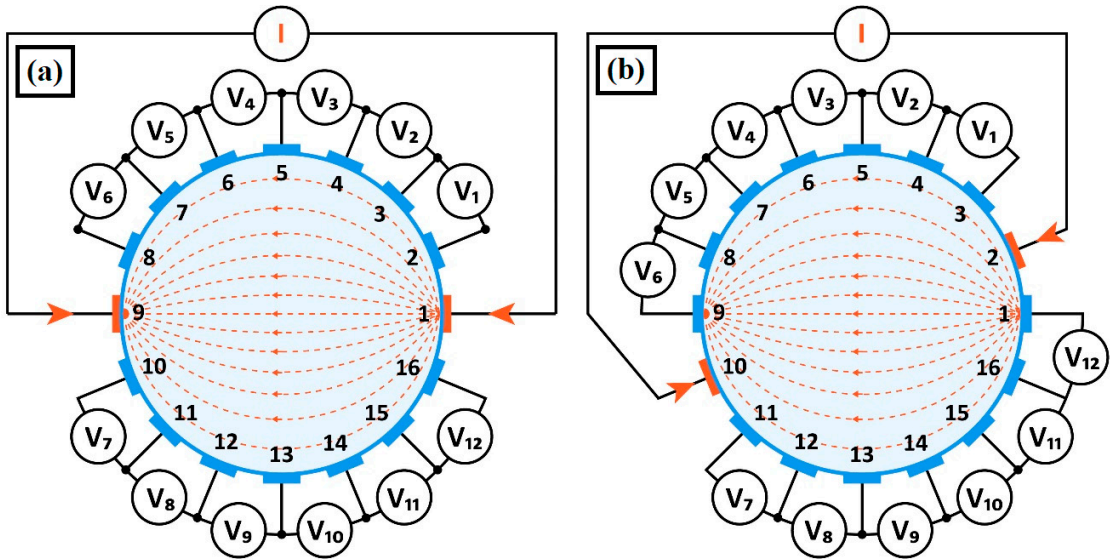
179   **Figure 5.** Voltage measurement method

180

181   Input data for the image construction algorithm are voltage measurements made between
182   adjacent electrodes. Measurements made on electrodes with an attached excitation source are omitted
183   due to unknown voltage drop between these electrodes and the tested area. For a system of n = 16
184   electrodes and any projection angle, n - 3 = 12 independent measurements can be obtained. Thus, the
185   full number of voltages measurable between neighboring voltage electrodes at n / 2 = 8 angles is:
186   (n - 3) (n / 2) = 12 · 8 = 96. The method of measuring the inter-electrode voltages shown in Figure 5

187   corresponds to the first and the second projection angle. For subsequent angles, sequential switching
188   of the power supply and measurement circuit to the neighboring electrodes takes place.

189   For a system of n = 32 electrodes and any angle of projection, n - 3 = 28 independent
190   measurements can be obtained. Hence the full number of possible independent measurements of
191   voltages between neighboring voltage electrodes at n / 2 = 16 angles is: (n - 3) (n / 2) = 28 * 16 = 448.

192   Potential values of electrodes depend on the current distribution within the region, and thus also
193   on the distribution of conductivity. The algorithm of computer image reconstruction is looking
194   iteratively for such a distribution of conductivity, for which the calculated values of inter-electrode
195   voltages are as close as possible to the corresponding measurement values.

196   The measured voltage is generally a voltage drop on the two impedances of the electrodes and
197   the impedance of the object. The voltage drop on the impedances of the spot electrodes can be omitted
198   due to the high impedance of the measuring system. In the case of surface electrodes, the potential
199   decrease at the electrode is very low, the tested object has low conductivity, while the electrode has
200   a high conductivity. Therefore, the voltage drop is negligible, the surface impedance coefficient of the
201   electrode tends to zero (it is negligibly small), but it is programmatically included in the
202   reconstruction process. The contact impedance is included in the model, but has a limited effect on
203   the measurement.

204   Voltage drops are measured on the surface of the tested object, so it is a non-invasive method.
205   After applying the power source in the wall, current starts flowing, which has a higher value closer
206   to the shore and the power source. The further away from the electrodes, the more the current flow
207   is getting smaller (tends to zero). This is the factor that causes the reconstruction to be more optimal
208   closer to the measuring electrodes, the further away from the electrodes, the detection precision may
209   be lower (the reconstruction may be worse due to the current depth distribution). Therefore,
210   measurements on one edge usually give worse quality compared to measurements on two or more
211   edges. Sometimes, however, only one-sided measurement is possible.

212   The tested physical models of the wall parts contained 16 or 32 electrodes each for measuring
213   the wet wall. The electrodes were placed on both sides of the tested wall sample. Electrical impedance
214   tomography is based on the measurement of the potential difference. The ability to determine the
215   wall condition results from the unique conductivity value of each material. The necessary equipment
216   such as electrodes, meters, alternating current generator, multiplexer and a computer with LabVIEW
217   and EIT modules was used for the measurements. Figure 6 (a) and (b) shows the partially immersed
218   lightweight concrete block on which the surface electrodes are placed. It can be seen that in the
219   presented picture the block samples have 2x8 (a) and 2x16 (b) electrodes.

220

Sample with 2 x 8 electrodes	Sample with 2 x 16 electrodes

 |

 |
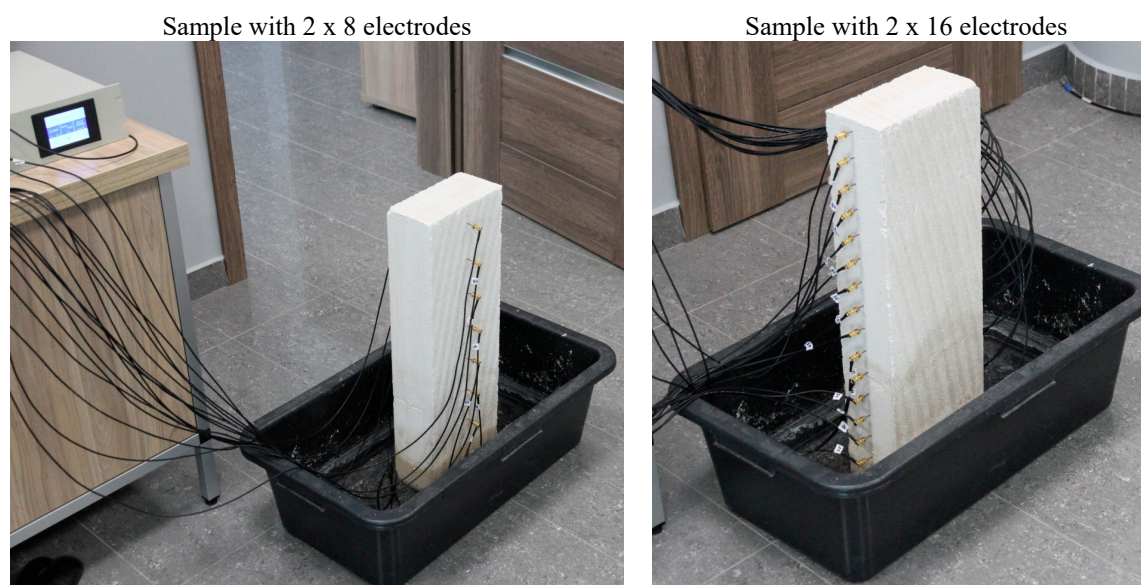
221   **Figure 6.** A tomographic laboratory to study the moisture inside the cellular lightweight concrete block

222   As mentioned before, a big problem related to the moisture content testing is the lack of a
223 method allowing to determine its spatial distribution without the need to take samples. The method
224 that enables this is electrical impedance tomography. It consists in evenly distributing the electrodes
225 on the tested object and ensuring a good contact of their surface with the tested surface.
226 Unfortunately, often the wall surfaces have a varied shape. Also, the building materials themselves,
227 such as brick or plaster, have a certain porosity, which makes measurement difficult. To ensure an
228 adequate flow of electric current between the individual electrode pairs, a special multilayer electrode
229 was developed.
230   Ensuring the proper contact of the electrodes with the wall is particularly important in testing
231 objects with an uneven as well as a rough surface. An example of the use of this type of electrodes is
232 the moisture condition investigation inside the masonry. The development of effective and efficient
233 measuring electrodes for impedance tomography has proved to be a serious challenge. In order to
234 ensure optimal contact between the electrode and the wall, an electrode with a flexible contact surface
235 and articulated mounting was designed. Figure 7 (a) shows how to attach a set of rubber electrodes
236 to the building wall. Figure 7 (b) shows a view of the electrode set, while Figure 7 (c) shows a
237 schematic view of the structure of a single rubber electrode.
238

239
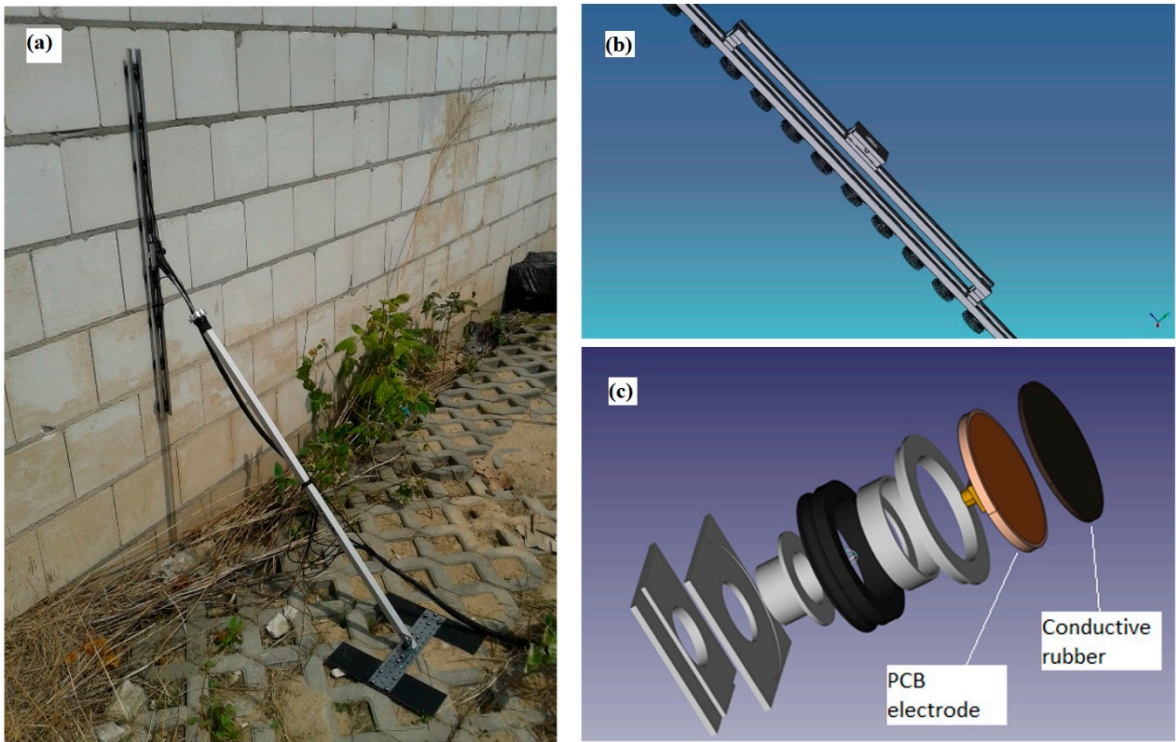
240   **Figure 7.** The concept of the electrodes

241   A complete electrode consists of three modules: a specific electrode, a PCB with a contact socket
242 and a fastening system. Mechanically, the modules are connected to each other by means of two
243 sleeves placed one inside the other. Before separating, they are secured by a collar placed on the
244 upper sleeve. The PCB is made of double-sided 1.54 mm thick laminate with an SMB1251B1-3GT30G-
245 50 socket.
246   From the active surface, the galvanic plate is connected by means of four leads with a specific
247 electrode made of electro-conducting silicone coated on the one hand in the galvanization process
248 with a copper layer. Pins and the copper layer allow contact between the PCB and the electrically
249 conductive silicone.

250   The specific electrode made of flexible electrically conductive silicone improves contact with the
251   surface of the tested object. This feature is particularly useful in examining objects with increased
252   porosity.
253   The third module is the tripod electrode mounting system. It is made of ASB in 3D printing
254   technology. The holder has two parallel channels that allow quick mounting on tripod profiles. The
255   element responsible for the elasticity of the mount is the rubber ring, which task is to adjust the
256   position of the electrode to the tested object surface, which aims to eliminate the unevenness and
257   pressing the electrode to the wall. The post-retrofit version is equipped with an additional 10 mm
258   thick shock absorber and a flexible connection between the conductive rubber and the PCB. As a
259   result, the electrodes adhere much better to uneven surfaces of the tested object. Newly designed
260   electrode systems have great potential in practical applications.

261   *2.2. Wall moisture tests with the use of the Gauss-Newton (GNM) method*

262   Figure 8 presents the results of tomographic imaging using the Gauss-Newton (GNM) method.
263   The presented reconstruction (b) deviates somewhat from the pattern image (a). The differences,
264   however, concern only the details of the contour of the moistened area. So you can use this method
265   to roughly estimate the moisture level and area.
266
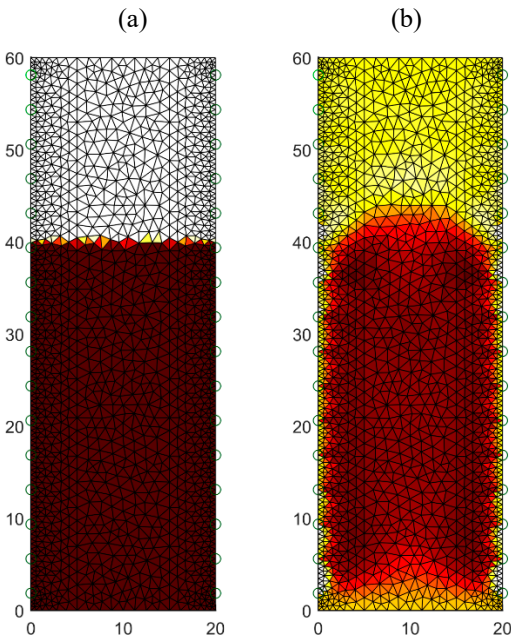
267   **Figure 8.** The geometrical model of the tested wet wall with 32 electrodes: (a) the pattern image, (b) the
268   image reconstructed by Gauss-Newton method

269   Figure 9 presents the spatial reconstruction of a wall fragment using the GNM method by means
270   of 32 measurement electrodes located around the object. Figure 9(a) is a reference image. Figure 9(b)
271   is the result generated by the use of GNM. Comparing both images, you can see differences in the
272   intensity of the color. Brighter colors of the reconstructed image indicate less intense moisture inside
273   the wall compared to the reference image.
274

275
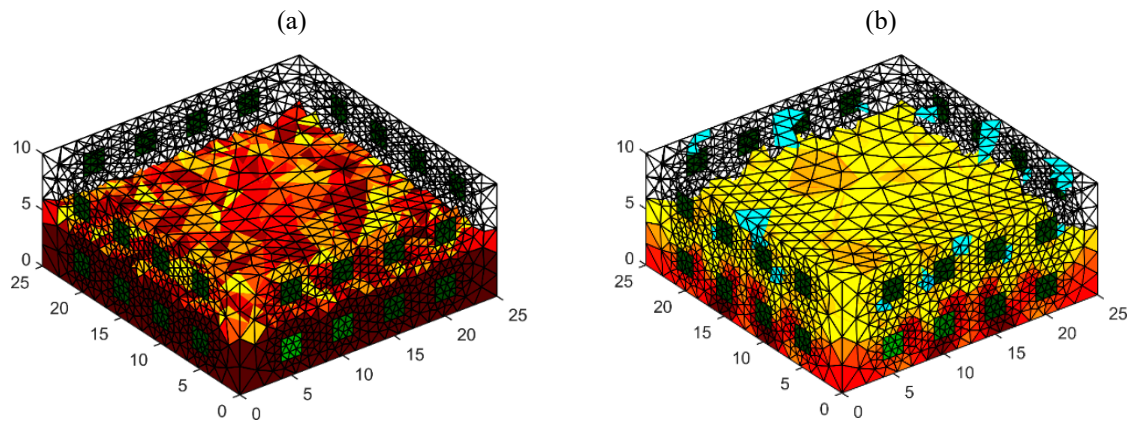
276   **Figure 9.** The geometrical model 3D with 4x8 electrodes – the image reconstruction: (a) pattern model, (b)
277   Gauss-Newton method with Laplace regularization

278   In Figure 10, we can see an example of a reconstruction of a damp concrete block using 32
279   electrodes located on both sides of the tested object. In order to solve the problem of the three-
280   dimensional finite element mesh was prepared. It can be noticed that surfaces of finite elements
281   which are localized near electrodes are small. Hence, the solution of the forward problem is precise.
282   The results obtained are similar to those obtained by placing 32 electrodes around the lightweight
283   concrete block with dimensions 10x40x90 cm. The reconstructed image deviates from the pattern with
284   the too low intensity of colors.
285
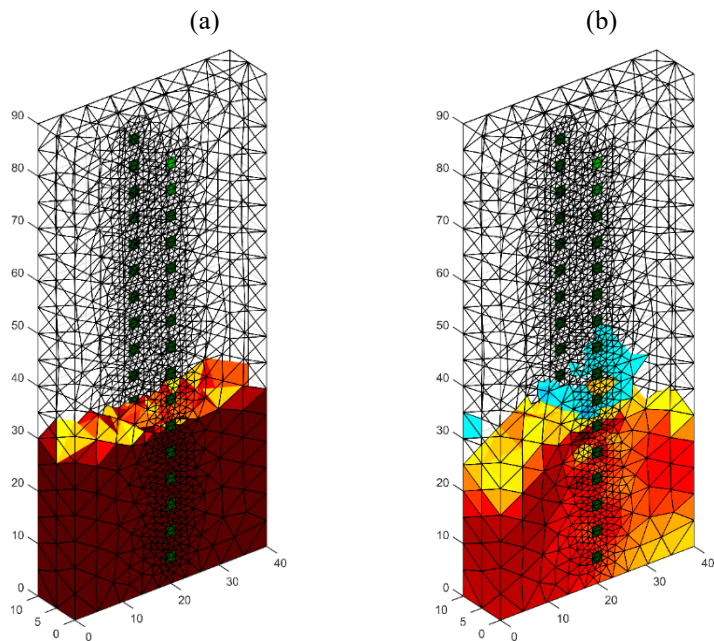
286   **Figure 10.** The geometrical model 3D with 2 x 16 electrodes – the image reconstruction: (a) pattern model,
287   (b) reconstruction created with the use of Gauss-Newton method with Laplace regularization

288   In Figure 11 two special models of the brick cube "wet" and "moist" with 2x8 electrodes are
289   presented. The image was reconstructed by Gauss-Newton method with Laplace regularization or
290   Tikhonov regularization.
291
292
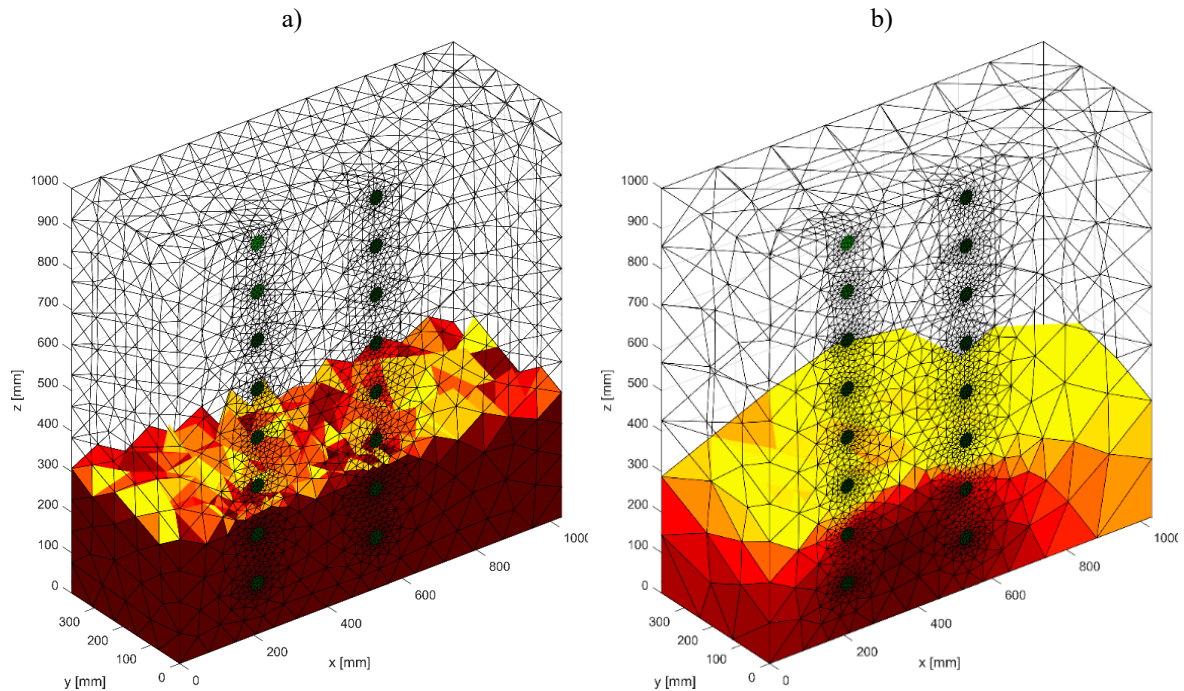
293   **Figure 11.** The geometrical model 3D with 2 x 8 electrodes – the image reconstruction: (a) pattern model,
294   (b) reconstruction created with the use of Gauss-Newton method with Laplace regularization

295   *2.3. Masonry humidity testing by the Least Angle Regression (LARS) method*

296   In order to obtain more accurate and stable reconstruction results in solving the inverse problem
297   in electrical tomography [19, 20, 21], a new solution based on the method of the least angle regression
298   was tested [27]. There are many methods to solve the optimization problem [26]. The statistical
299   methods can be used to reconstruct an image in electrical impedance tomography [28, 29].
300   The main objective of the tomography is to perform image reconstruction. During the
301   measurements, we can see that the measured values from some electrodes are strongly correlated
302   (due to the way of measurement). In this case, we have a multicollinearity problem. When the
303   independent variables (predictors) are correlated (collinear), then the matrix tends to a single matrix.
304   By means of the least squares method, we obtain large absolute values of some estimators with
305   unknown parameters. Forecasts based on this model are unstable. The most common approach is to
306   reduce the set of input variables (removing the same predictors that apply to multicollinearity). Then
307   we have a problem with the selection of predictor variables that will be included in the regression
308   model. For example, when comparing the AIC (Akaike Information Criterion) value for linear models
309   with different sets of predictors, we can choose the best model.
310   Another possible way to reduce the problem of multicollinearity between predictors depends
311   on the application of the least angle regression algorithm. This algorithm takes into account only
312   causal variables in the linear model (from the set of predictors, you should select the input variables
313   that have a direct impact on the response variable). In this case, the linear model is built by means of
314   step forward regression, where the best variable is added to the model in every step.
315   Let the linear system be described by the state equation

$$Y = X\beta + \varepsilon \tag{1}$$

316   where $Y \in R^n, X \in R^{n \times (k+1)}$ denote the observation matrices of response and input variables
317   respectively, $\beta \in R^{k+1}$ denotes the vector of unknown parameters. When the linear model (1)
318   contains the intercept, then the first column of matrix X is a column of ones. The object $\varepsilon \in R^n$ in the
319   linear system (1) presents a sequence of disturbances, which is usually defined as a vector of
320   independent identically distributed random variables with normal distribution $N(\tilde{0}, \sigma^2 I)$, which,

321   $\tilde{O} \in R^n$ is a zeros vector but $I \in R^{n \times n}$ is an identity matrix. The classical Least Square Method
322   depends on identification of unknown parameters $\beta = (\beta_0, \beta_1, \dots, \beta_k)$ in (1) by solution the task

$$\min_{\beta \in R^{k+1}} \|Y - X\beta\|^2 \tag{2}$$

323   If $\det(X^T X) \neq 0$, then the best unbiased linear estimator of unknown parameters β is

$$\hat{\beta} = \left(X^T X \right)^{-1} XY \tag{3}$$

324   The problem is often when $X^T X$ is singular.
325   The following is a short version of the least angle regression algorithm as the workflow. An extended
326   version of LAR has been presented in [30].

1.   The predictors should be standardized. The intercept β_0 in expression (1) is equal a mean of
     the response variable and we put $\beta_1 = \beta_2 = \dots = \beta_k = 0$. Active set A (set of predictors) is
     empty.
2.   Calculate the residuals $r = Y - \beta_0 - X_{(A)}\beta_{(A)}$ for the linear model with all predictors from
     active set A. Determine the predictor X_j (which is not in active set) most correlated with
     residuals r and attach to the active set A.
3.   Move coefficient β_j from 0 towards its least-squares coefficient $\langle X_j, r \rangle$ until some other
     competitor X_k has a much correlation with the current residuals as does X_k.
4.   Move β_j and β_s in the direction defined by their joint least square coefficient of the current
     residual on $\langle X_j, X_s \rangle$ until some other competitor X_l has a much correlation with the current
     residual.

   Go to step 2 and continue in this way until all k predictors have been entered.

339   *2.5. Masonry humidity testing by the ElasticNet method*

340   Another way to determine the linear regression when the input variables are collinear depends
341   on the solution of the task

$$\min_{(\beta_0, \beta') \in R^{k+1}} \frac{1}{2n} \sum_{i=1}^{n} \left(y_i - \beta_0 - x_i \beta' \right)^2 + \lambda P_\alpha \left(\beta' \right), \tag{4}$$

342   where $x_i = (x_{i1}, \dots, x_{ik})$, $\beta' = (\beta_1, \dots, \beta_k)$ for $1 \leq i \leq n$ and P_α is an elastic net penalty given by

$$P_\alpha \left(\beta' \right) = \left(1 - \alpha \right) \frac{1}{2} \|\beta'\|_{L_2} + \alpha \|\beta'\|_{L_1} = \sum_{j=1}^{k} \left(\frac{1-\alpha}{2} \beta_j^2 + \alpha |\beta_j| \right) \tag{5}$$

343   We see that the penalty is a linear combination of norms L_1 and L_2 of unknown parameters
344   β'. The introduction the penalty function dependent from parameters to the objective function allows
345   to shrink the estimators of unknown parameters.
346   The parameter λ in the task (4) denotes the coefficient of penalty, but the parameter $0 \leq \alpha \leq 1$
347   creates the compromise between LASSO (Least Absolute Shrinkage and Selection Operator) and
348   ridge regression. The ridge regression ($\propto = 0$) is called Tikhonov regularization [31] and is one of the
349   most commonly used for regularization of linear models. LASSO ($\propto = 1$) was introduced by Roberta
350   Tibshirani [32, 33]. This method performs the variable selection and regularization in linear statistical
351   models [34, 35]. For the ridge regression, the penalty is calculated in the norm L_1 but for LASSO in
352   L_2. Difference between ridge regression and LASSO is symbolic, only the norms are changed. The
353   ridge regression shrinks coefficients for correlated predictors towards each other. When the
354   correlated predictors depend on any latent factor, then ridge regression allows to uniformly
355   distribute the strength of latent factor on these predictors. Whereas LASSO is indifferent to correlated
356   predictors. This method allows to determine the preferred predictor and to ignore the rest. By
357   applying LASSO method we obtain a model, where the many coefficients to be close to zero, and as
358   a result, we receive a sparse model. The elastic net is a connection of ridge regression and LASSO [36,

359 37]. Choosing the appropriate α we may create the compromise between ridge regression and
360 LASSO.

361 By solution the task (4) for fixed λ and α we estimate the unknown parameters of the linear
362 system (1), where predictors are correlated. Then the prediction based on model (1) is given by the
363 formula $\hat{Y} = X\hat{\beta}$, where the vector of estimators of unknown parameters $\hat{\beta} = (\hat{\beta}_0, \hat{\beta}_1, \dots, \hat{\beta}_k)$ is
364 estimated by solution the task (4).

2.6. Masonry humidity testing by the Gauss-Newton method

366 In the electrical impedance tomography in the reconstruction of the image, the so-called
367 Generalized Tikhonov regularization is very often used. In the literature on the subject, this method
368 is also known as the Gauss-Newton algorithm in a generalized form.

369 The Gauss-Newton method is based on the application of the least squares method in which the
370 matrix $Z^{(l)}$ fulfills the role of matrix X (first partial derivatives relative to fixed approximations $\beta^{(l)}$
371 and observed values of independent variables), and the role of the vector y (observation of the
372 dependent variable) vector $e^{(l)}$. It is a vector of differences between the empirical values of the
373 dependent variable and the lth of its approximations $f(x_t, \beta^{(l)})$.

374 The Gauss-Newton algorithm is used to estimate the structural parameters of non-linear models.
375 The general form of the non-linear function is presented below:

$$y_t = f(x_t, \beta) + \varepsilon_t \qquad (10)$$

376 where:
377 y_t – observations of the explanatory variable,
378 $x_t = [x_t]$ – P vector of observations for explanatory variables,
379 $\beta_t = [\beta_j]$ – K vector of structural parameters,
380 ε_t – implementations of random elements (we assume that random components are
381 uncorrelated, have an average of zero and equal, positive and finite variance).

382 In the Gauss-Newton method, the reconstruction of the internal image of the investigated object
383 is related to the determination of the global minimum of the fitness function. In order to carry out
384 quantitative considerations, we assume that the tested object is polarized with an alternating low-
385 frequency current. Then, the electrical material properties can be described by a function with real
386 values. In this case, in the generalized Laplace equation, we neglect the word proportional to the
387 frequency, and this function can be equated with the electrical conductivity (real isotropic admittivity
388 case).

2.7. Masonry humidity testing by the neural imaging

390 In order to solve the problem of non-invasive imaging of the interior of moist walls, the method
391 of electrical tomography in connection with artificial neural networks was also used. So far,
392 tomographic and neural networks methods have not been widely disseminated in the assessment of
393 the wall. The reason is the low resolution of the reconstructed image and the low accuracy of
394 mappings [7].

395 To increase the resolution of tomographic reconstructions depicting the degree of internal
396 humidity of walls, a new method was developed based on a set of many separately trained neural
397 networks. The number of neural networks corresponds to the 3D resolution of the lattice dividing the
398 inside of the wall into individual pixels. In the presented experiment a lightweight concrete block
399 with dimensions 10x40x90 cm was used, which was divided into 8099 points.

400 Using a device called a multiplexer, in short intervals, the tomographic system generates 192
401 values of voltage drops readings between different electrode pairs. These are the input data for the
402 neural network system. The neural networks are designed in such a way that on the basis of an input
403 vector containing 192 elements, each of the 8099 neural networks generates the value of a single pixel
404 of the output image.

405 Figure 12 shows the mathematical form of the neural model used during simulation
406 experiments. At the model input, there are 192 electric signals generated by 16 electrodes.

407
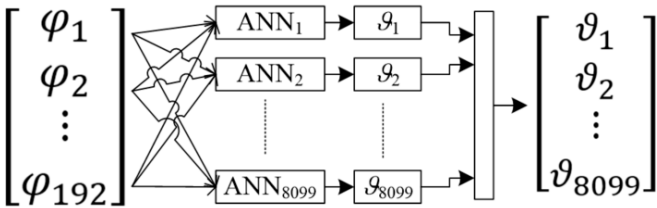
408   **Figure 12.** The scheme of converting electrical signals into the image pixels

409   The same input vector is the basis for training 8099 separate artificial neural networks (ANN).
410 In this way, from a vector of 192 variables representing electrical values, a set of neural networks
411 creates a complete lattice of the lightweight concrete block image. The output image is created by
412 assigning colors to the output values of each pixel. The transformation method is shown in Figure 13.
413

414
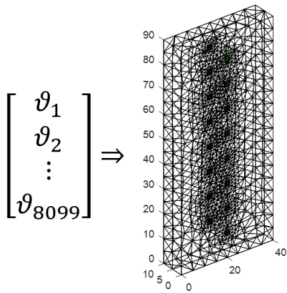
415   **Figure 13.** The way of converting a real number vector into the lightweight concrete block's spatial
416   image

417   Each of the 8099 neural networks had a multi-layered perceptron structure with 10 neurons in
418 the hidden layer. The scheme of a single perceptron is shown in Figure 14.

419
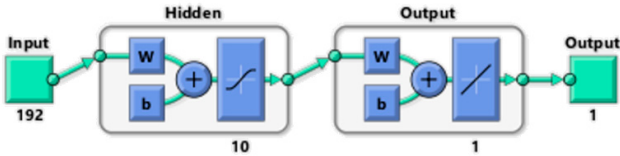
420   **Figure 14.** Structure of the selected multi-layer perceptron

421   In order to collect data necessary to train the neural network, physical and mathematical models
422 were developed. The finite element method was used for this. Based on a mathematical model, a data
423 set was generated. After that, it was used to train the neural network system.
424   To train the mentioned above neural network, a collection of 6,140 historical cases was used (see
425 Table 1). The main set of data has been divided into 3 separate subsets: a training set, validation set,
426 and testing set, in the proportions of 70%, 15%, 15%. This method of data preparation has been used
427 for all 8099 neural networks.

428   **Table 1.** Training results for one of 8099 neural networks

	🐞 Samples	🗒 MSE	🖉 R
🛡 Training:	4298	5.31979e-6	9.99983e-1
🟢 Validation:	921	1.68249e-5	9.99947e-1
🔴 Testing:	921	2.03645e-5	9.99934e-1

429
430
431   The highest Mean Squared Error (MSE) concerned the testing set and was 0.000020364. In the
432 case of validation set, a slightly smaller error was noted. Mean Squared Error is the average squared
433 difference between outputs and targets. Lower values mean better performance. Zero means no error

434   (excellent performance). The training set was trained with the lowest training error, which is the most
435   common and correct situation. A low MSE error in the training set results from better network
436   adaptation to training cases. Another indicator of the quality of network learning was R (Regression).
437   An R value of 1 means a close relationship between pattern and output, 0 a random relationship. In
438   all three cases of data sets (learning, validation, and testing), R was close to 1. This also applies to the
439   test and validation set, which is particularly valuable. Values close to 1 indicate a good match of the
440   results obtained by the network (output vectors) to the patterns included in the individual sets
441   (training, validation, and testing).
442   Good indicators (MSE and R) for the training set show the lack of overtraining effect and the
443   ability of the network to knowledge generalization (i.e., correct conversion of input data to output
444   information not only for learning cases).

3. Results

446   This chapter presents the results of wall humidity tests by EIT tomography in combination with
447   the following machine learning algorithms: Least Angle Regression (LARS), ElasticNet and Artificial
448   Neural Networks. The root mean square error of prediction (RMSE) indicator was used to quantify
449   the quality of the reconstructions obtained using simulation models.
450   Let vector $x = (x_1, \dots, x_n)$ presents the pattern, which should be reconstructed. After
451   reconstruction we obtain the vector, $\hat{x} = (\hat{x}_1, \dots, \hat{x}_n)$ which contains the expected values of
452   reconstruction of explored object. The root mean square error of prediction was determined by the
453   formula (11).

$$RMSE = \sqrt{\frac{1}{n} \sum_{i=1}^{n} \left(x_i - \hat{x}_i\right)^2} \tag{11}$$

454   In the further part of this paper two variants of images were compared: 2D and 3D. The 2D
455   image lattice consisted of 2908 pixels, while the 3D grid consisted of 8099 pixels. Thus in the first case
456   (2D) n = 2908, while for the 3D variant n = 8099.
457   All results enabling the comparison of LARS, ElasticNET and ANN methods were obtained
458   thanks to the use of computer simulation methods. The simulated data has been used with added
459   noise to SNR = 14 dB. This noise parameter was calculated for a given measurement system
460   configuration and includes measurement patterns and electrode positions. SNR is defined in terms
461   of power as a signal to noise ratio.

3.1. Results of wall moisture tests obtained using the Least Angle Regression (LARS) method

463   Figure 15 presents one of the results of tomographic imaging using the LARS method. The input
464   data was obtained thanks to the use of an EIT tomograph equipped with 16 electrodes (2x8). Intense
465   colors indicate areas with higher humidity. It can be seen, the obtained reconstructive image (in the
466   middle) is very close to the reference image (left). The difference image (right) indicates small
467   deviations of the grid points in the reconstructed image from the reference image. The colors in the
468   images reflect the conductance of the individual pixels that each image consists of. The lack of color
469   in the original and reconstruction images testify to the lack of moisture. RMSE for a 3D sample with
470   the use of LARS is 0.0298.
471
472
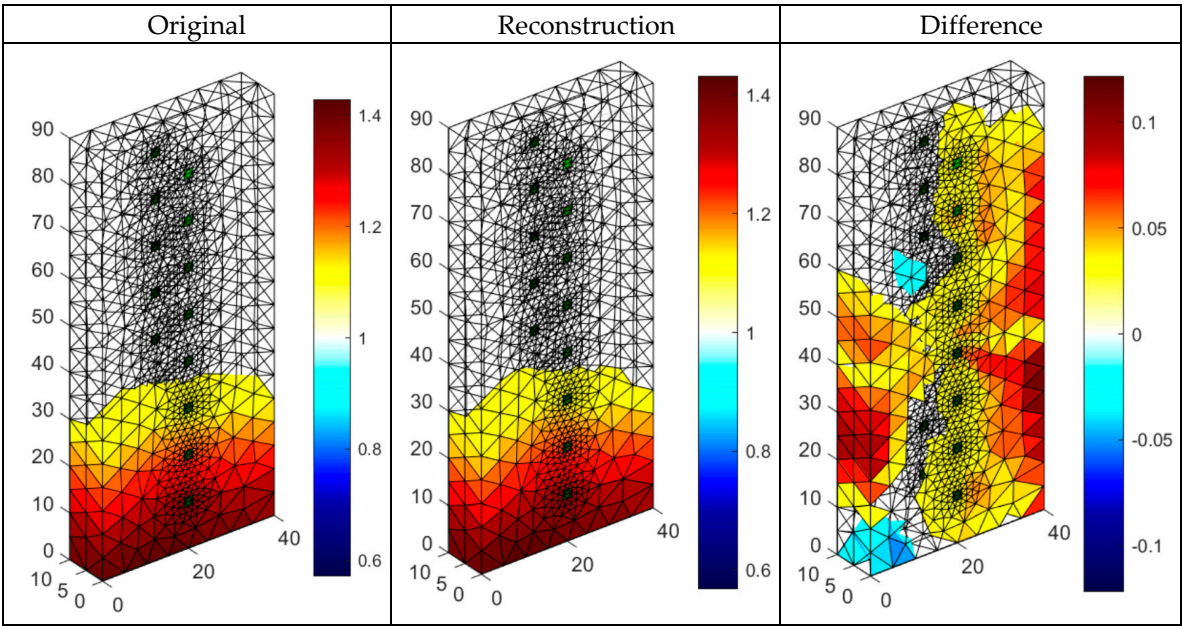
473   **Figure 15.** The result of Least Angle Regression (LARS) moisture testing of the lightweight concrete block for the
474   case of 2x8 electrodes

475   Figure 16 shows a case analogous to the previous one, which was presented in Figure 15, but
476   this time a cellular concrete sample with slightly different dimensions (10x20x60 cm) was used. The
477   reconstruction was carried out in 2D. RMSE for a 2D sample with the use of LARS is 0.122599.
478

479
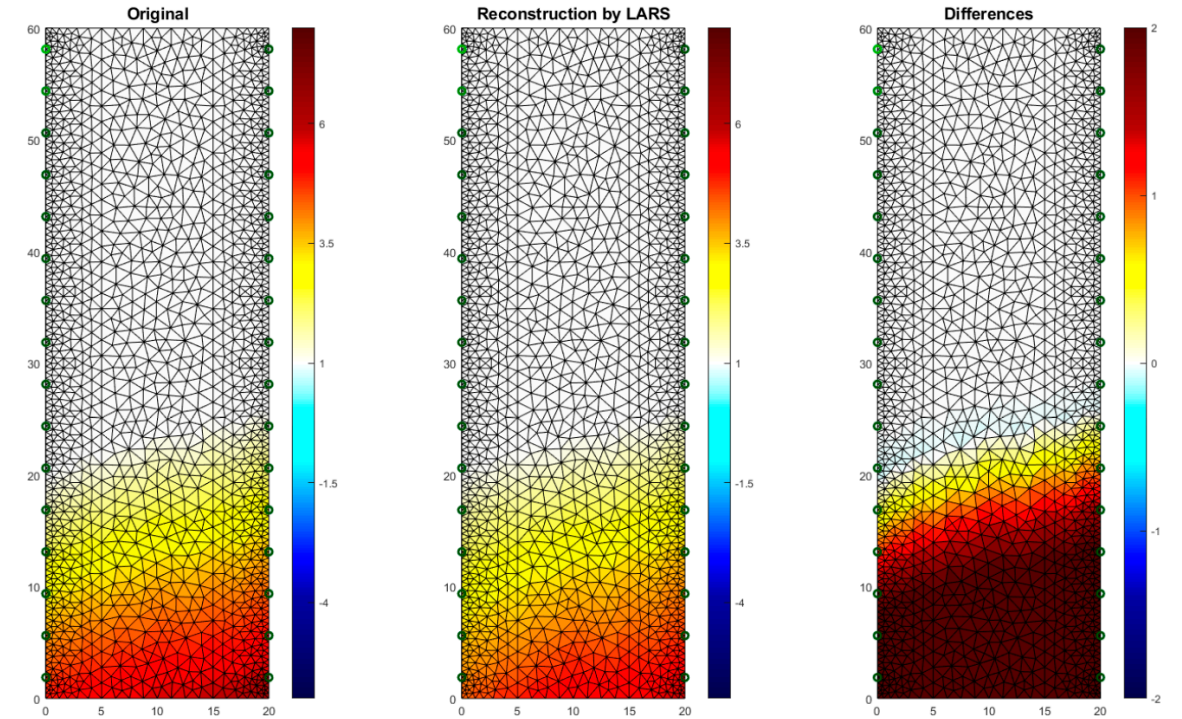
480   **Figure 16.** The result of Least Angle Regression (LARS) moisture testing of the lightweight concrete block
481   for the case of 2x16 electrodes

482   *3.2. Results of wall moisture tests obtained using the ElasticNet method*

483   Figure 17 presents an example of a tomographic 3D imaging result using the ElasticNet method.
484   The input data was obtained thanks to the use of an EIT tomograph equipped with 16 electrodes
485   (2x8). Intense colors indicate higher humidity spots. It can be seen, the obtained reconstructive image

486　(middle image) is comparable to the reference image (left). The image of residuals (right) indicates
487　the occurrence of deviations of the grid points of the image reconstructed from the reference image.
488　The lack of color and shades of blue in the original and reconstruction images mean the lack of
489　moisture. RMSE for a 3D sample with the use of ElasticNet is 0.0365.
490
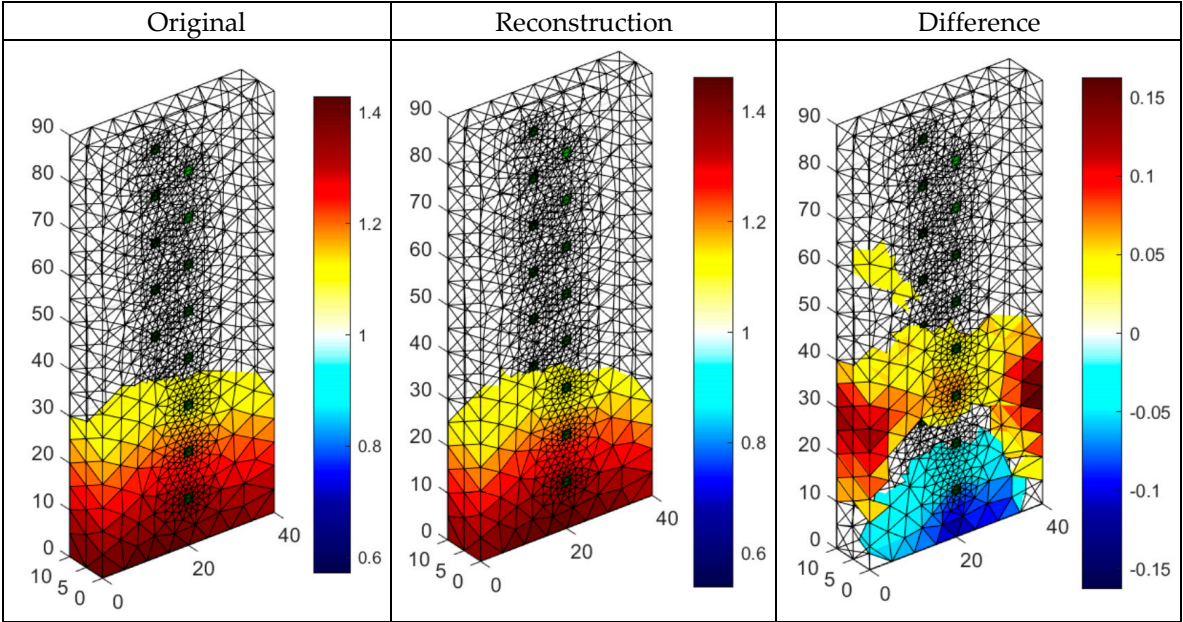
491　**Figure 17.** The result of ElasticNet moisture testing of the lightweight concrete block for the case of 2x8
492　electrodes

493
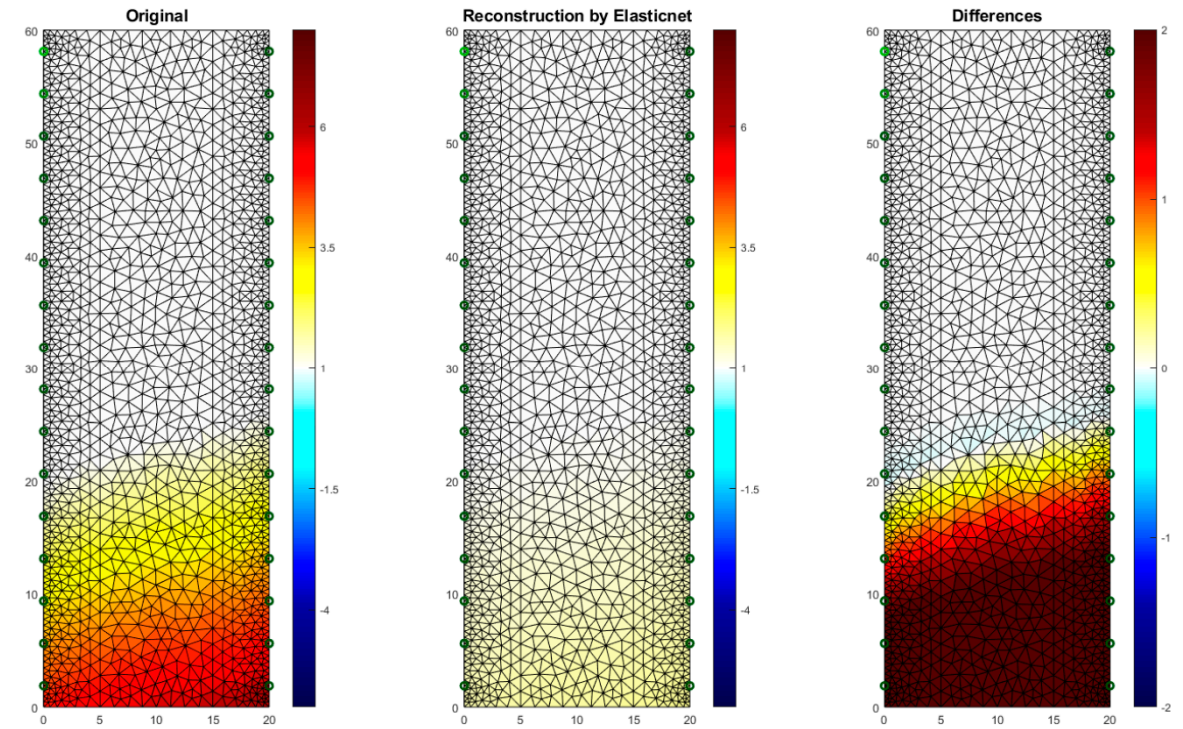
494　**Figure 18.** The result of ElasticNet moisture testing of the lightweight concrete block for the case of 2x16
495　electrodes

496　　　　Figure 18 presents an example of a tomographic imaging result using the ElasticNet method.
497　The input data was obtained thanks to the use of an EIT tomograph equipped with 32 electrodes
498　(2x16). Intense colors indicate higher humidity spots. It can be seen that the obtained reconstructive

499   image (middle image) reproduces the reference image (left) poorly. The image of differences (right)
500   indicates the occurrence of significant deviations of the grid points of the image reconstructed from
501   the reference image. RMSE for a 2D sample with the use of ElasticNet is 0.282520. Compared with
502   LARS, ElasticNet showed the lower quality (higher RMSE) of reconstruction in this case.

503   *3.3. Results of wall moisture tests obtained using the neural imaging*

504   Figure 19 presents the results of neural imaging in conjunction with the EIT. Conductive
505   (positive) areas are shown in shades of red. Non-conductive (negative) areas are shown in blue or
506   they are transparent. Comparing the pattern of the damp block (original) with the output image, we
507   conclude that the accuracy of the imaging is very high. The right image shows the absolute
508   (numerical) differences in the values of individual pixels are minimal. They do not exceed +/- 0.05. It
509   can be seen that the results obtained by the neural imaging method are comparable to the results
510   obtained by both previous methods. RMSE for a 3D sample with the use of ANN is 0.010819 so the
511   quality is better than LARS and ElasticNET.
512
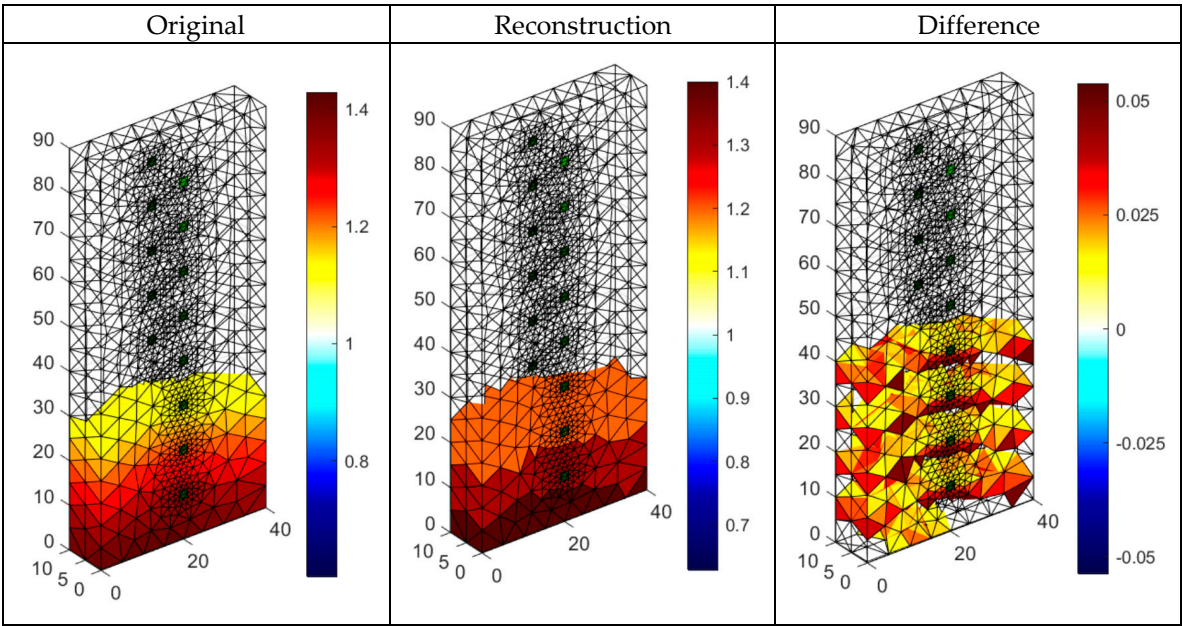
513   **Figure 19.** The result of Artificial Neural Network system (ANN) moisture testing of the lightweight
514   concrete block for the case of 2x8 electrodes

515   Figure 20 shows an analog measurement of a 2D sample with two rows of electrodes on both
516   sides of the block (2x16). Noteworthy is the small amount of colored pixels in the differential image.
517   This indicates high quality imaging, which is confirmed by the low RMSE index, which in this case
518   equals 0.106301.
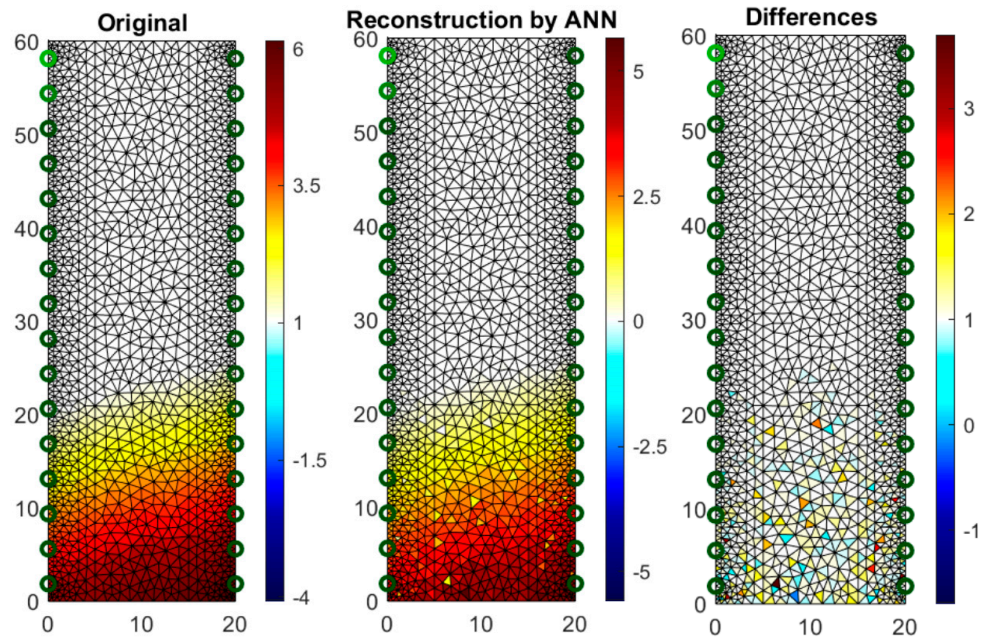
Figure 20. The result of Artificial Neural Network system (ANN) moisture testing of the lightweight concrete block for the case of 2x16 electrodes

3.4. Moisture test of real object

Figure 21 shows the results of the reconstruction of a block of cellular concrete immersed in water, using a system of artificial neural networks. Reconstructions based on data obtained from real objects, in contrast to simulation experiments based on numerical models are the most difficult type of test for tomographic systems. The first image on the left is the result of the direct processing of the tomographic data with the use of ANN. The ambiguous visual effect is caused by noise in the value of the input vector, which in the case of real objects is basically unavoidable.

To show the results in a way that visually identifies the moisture area, the input vector was subjected to a denoising procedure using denoising stacked autoencoders [38]. The results of denoising were presented in the middle image entitled "First denoising". Finally, the output image was subjected to one more processing using a filtering script whose objective was to cut off the output values, which obviously exceeded the acceptable range. The filtering effects are shown in the image entitled "Second denoising". Finally, it was possible to reduce the number of incorrectly reconstructed pixels in the central part of the sample, but it was not possible to obtain a "clean image".

Denoising of tomographic data is an important issue because it affects the results of reconstruction. Due to the complexity of this subject, it may be the subject of separate studies aimed at improving the quality of tomographic images.
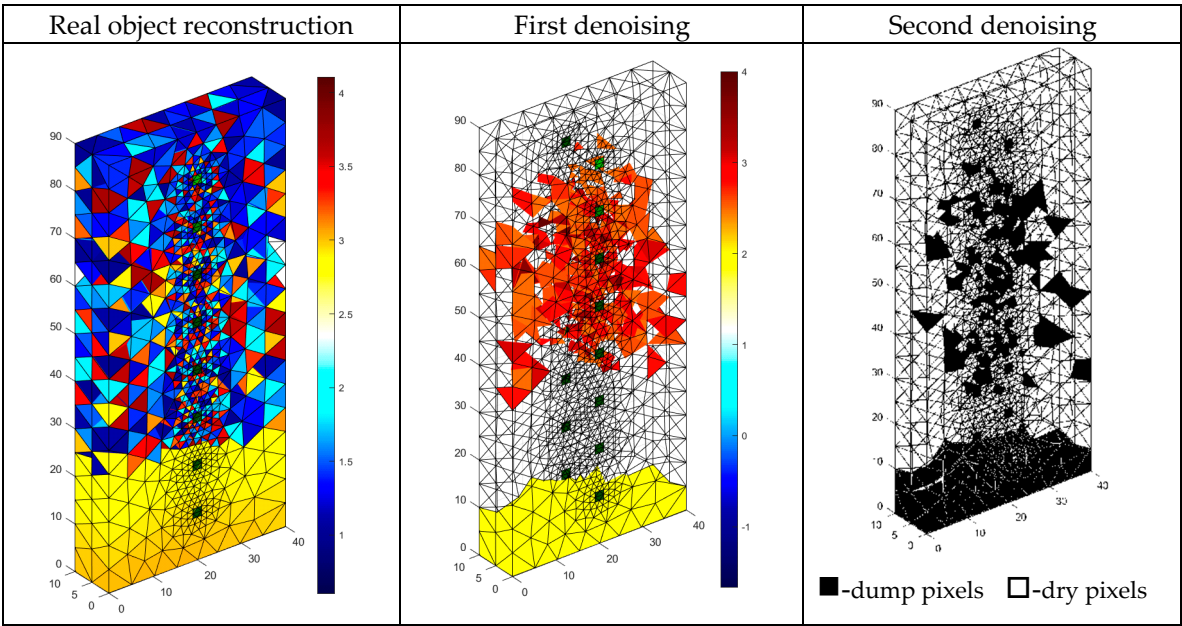
Figure 21. The result of the real object ANN moisture testing of the lightweight concrete block for the case of 2x8 electrodes

4. Discussion

The imaging results presented in the previous chapter show great application possibilities of the machine learning algorithms combined with EIT. The analysis involved 3 methods and algorithms converting input vectors (values of voltage drops) into reconstructed images reflecting the conductance: Least Angle Regression (LARS), ElasticNet and Artificial Neural Networks (ANN). Of the above methods, the best results were obtained using ANN. However, the LARS method in terms of fidelity representation is very similar to ANN.

Table 2 presents a summary of the RMSE values for cases of 2D and 3D imaging in relation to 3 methods tested: ANN, LARS and ElasticNET. The lowest values of the indicators, demonstrating the highest imaging quality, were obtained for ANN.

Table 2. Comparison of the quality of different imaging methods

Method	RMSE	
	2D samples	3D samples
ANN	0.106301	0.010819
LARS	0.122599	0.029800
ElasticNET	0.282520	0.036500

Both LARS and ANN can be successfully used in the EIT tomography dedicated to the reconstruction of moisture in masonries and building walls. In comparison to other, previously used algorithms, these methods allow obtaining precise images with sufficient resolution to perform an effective and error-free analysis of the moisture content of the walls. It is worth noting that taking into account the possibilities of spatial image creating, the LARS and ANN methods are more reliable than invasive methods requiring the sampling of masonry.

It is also important that the presented algorithms, used in connection with the EIT system and specially designed electrodes, have large application possibilities. Their basic advantages are functionality, reliability, measurement accuracy and reasonable price. The method is universal due to the possibility of applying to masonry and walls of the various structure, thickness and moisture level. An important role is also played by the speed of the computed tomography scanner. Output images are obtained in real time.

568   The electrical impedance tomography proposed in this article enables the creation of a new non-
569 invasive technique for measuring the humidity of building walls. The EIT has been used to determine
570 the conductivity distribution in specially constructed wall models made of light concrete blocks or
571 bricks. The finite element method implemented in the EIDORS environment has been used to solve
572 the problem. The numerous different lattices were used in the presented numerical models. The
573 analyzed measurement systems contained various electrode distributions. Thanks to this, it is sure
574 that the obtained results are not accidental but repeatable while maintaining similar conditions of the
575 measurement environment.
576   The research has provided new and promising results. Future work will be continued thanks to
577 the use of regularization techniques in the optimization process and the hybrid measurement system.
578 These types of hybrid measuring system should be even more reliable in practical applications. It
579 would also be interesting to extend the experimental measurements over time by monitoring the
580 walls at regular intervals. Thanks to this, it would be possible to estimate the speed of spreading the
581 moisture inside walls, as well as its sources and propagation directions.

582 **5. Conclusions**

583   The main goal of the work was to analyze the solution based on electrical tomography to study
584 the moisture of walls. Non-destructive methods and algorithms have been analyzed and compared,
585 which allow estimation of humidity also inside the wall. A new concept of a non-destructive system
586 based on electrical tomography has been presented. For research purposes, specially designed
587 electrodes were used, which were placed on the tested lightweight concrete and brick blocks. Three
588 machine learning algorithms were tested: Least Angle Regression (LARS), ElasticNet and Artificial
589 Neural Networks.
590   It was found that all four methods are suitable for practical applications in EIT tomography
591 dedicated to the detection of moisture in building walls, however, the best results were obtained
592 using the LARS method and the specially designed multi-ANNs system. A characteristic feature of
593 the analyzed solution is the division of the modeled object using a specially developed mesh for a set
594 of elements. The color of each individual mesh element corresponds to the conductance value (in the
595 EIT tomograph). Thanks to this approach the number of information determining the reconstructive
596 picture was large enough to guarantee a sufficient resolution of tomography imaging.
597   The presented research results contain relevant information that may contribute to the
598 acceleration of the development of computational intelligence and machine learning methods in EIT.
599 The research contributes to the improvement of the tomographic imaging efficiency of known
600 methods in the aspect of algorithms for processing input information (electrical quantities) into
601 images. In addition, enriching an input vector with values other than electrical is an easy way to
602 develop new, intelligent tomographic hybrid systems.

603 **Author Contributions:** Tomasz Rymarczyk has developed a research project and methods for testing the
604 moisture of walls using electrical tomography. As an expert in the work of tomography, he was the originator
605 of most machine learning concepts presented in this study. Grzegorz Kłosowski carried out research especially
606 in the field of artificial neural networks and was responsible for the substantive and editorial aspects of the
607 presented paper. Edward Kozłowski has implemented statistical methods and developed mathematical models
608 descriptions.

609 **Acknowledgments:** The authors would like to thank the authorities and employees of the Institute of
610 Mathematics, Maria Curie-Skłodowska University, Lublin, Poland for sharing supercomputing resources.

611 **Conflicts of Interest:** The authors declare no conflict of interest.

612 **References**

613 1.   Kic, P. Influence of moisture on thermal properties of walls in basements of buildings, *Engineering for Rural*
614   *Development - International Scientific Conference*, **2017**, vol. 24, pp. 492-495.
615 2.   Prejza, M.; Kic, P. Reduction of moisture in basements of buildings, *Engineering For Rural Development -*
616   *International Scientific Conference*, **2016**, pp. 68-73, Academic Search Complete, EBSCO*host*, viewed 19 June
617   2018.

618 3. Zhang, Z. A review of rising damp in masonry buildings. Advanced Polymer and Composite Research,
619   **2010**.
620 4. Walker, R.; Pavía, S. Thermal and moisture monitoring of an internally insulated historic brick wall,
621   *Building And Environment*, **2018**, 133, pp. 178-186, ScienceDirect, EBSCOhost, viewed 19 June 2018.
622 5. Hall, C.; Hoff, W. D. Rising damp: capillary rise dynamics in walls. In: *Proceedings of the Royal Society of*
623   *London A: Mathematical, Physical and Engineering Sciences*. The Royal Society, **2007**. p. 1871-1884.
624 6. Rybak, G.; Chaniecki, Z.; Grudzień, K.; Romanowski, A.; Sankowski, D. Non–invasive methods of
625   industrial process control, *Informatyka, Automatyka, Pomiary w Gospodarce i Ochronie Środowiska*, **2014**, 4/3
626   41–45
627 7. Rymarczyk, T., Kłosowski, G. Application of neural reconstruction of tomographic images in the problem
628   of reliability of flood protection facilities. *Eksploatacja i Niezawodnosc – Maintenance and Reliability*, **2018**; 20
629   (3): 425–434, http://dx.doi.org/10.17531/ein.2018.3.11.
630 8. Rymarczyk, T.; Tchórzewski, P.; Adamkiewicz, P.; Duda, K.; Szumowski, J.; Sikora, J. Practical
631   Implementation of Electrical Tomography in a Distributed System to Examine the Condition of Objects,
632   *IEEE Sensors Journal*, vol. 17, Issue:24, **2017**, pp. 8166-8186, DOI: 10.1109/JSEN.2017.2746748.
633 9. Berowski, P.; Filipowicz, S. F.; Sikora, J.; Wójtowicz, S. Determining location of moisture area of the wall
634   by 3D electrical impedance tomography, *4th World Congress in Industrial Process Tomography*, **2005**, 214-219.
635 10. Borsoi, R. A.; Aya, J. C. C.; Costa, G. H.; Bermudez, J. C. M. Super-resolution reconstruction of electrical
636   impedance tomography images. *Computers & Electrical Engineering*, **2018**, *69*, 1–13.
637   https://doi.org/10.1016/J.COMPELECENG.2018.05.013
638 11. Corbellini, S.; Parvis, M.; Grassini, S.; Piantanida, M.; Consalvi, F.; Gigante, G.; Meddi, F. Electrical
639   tomography for the monitoring of water moisture in painted walls and ceilings, *2010 IEEE International*
640   *Instrumentation And Measurement Technology Conference*, I2MTC 2010 - Proceedings, no. 2010 IEEE
641   International Instrumentation and Measurement Technology Conference, I2MTC 2010 - Proceedings, p.
642   975-980. Available from: 10.1109/IMTC.2010.5488069. [19 June 2018].
643 12. Suryanto, B.; Saraireh, D.; Kim, J.; McCarter, WJ.; Starrs, G.; Taha, HM. Imaging water ingress into concrete
644   using electrical resistance tomography, *INTERNATIONAL JOURNAL OF ADVANCES IN ENGINEERING*
645   *SCIENCES AND APPLIED MATHEMATICS*, **2017**, no. 2, p. 109.
646 13. Woelfl, G.; Lauer, K. The Electrical Resistivity of Concrete with Emphasis on the Use of Electrical Resistance
647   for Measuring Moisture Content. *Cement, Concrete and Aggregates*, **1979**, Vol. 1, No. 2, pp. 64-67.
648 14. ENOSTA, company established in 1989. Available online: http://www.enosta.pl (access on 7 February
649   2018).
650 15. Gjørv, O. E.; Vennesland, Ø.; El-Busaidy, A. H. S. Electrical Resistivity of Concrete in the Oceans. In
651   *Proceedings 9th Annual Offshore Technology Conference*, **1977**, Houston, Texas.
652 16. Hoła, J.; Matkowski, Z.; Schabowicz, K.; Sikora, J.; Nita K.; Wójtowicz S. Identification of Moisture Content
653   in Brick Walls by means of Impedance Tomography, *COMPEL*, **2012**, 31/6 1774-1792.
654 17. Trochonowicz, M. Moisture in buildings objects. Humidity testing problems. Lublin University of
655   Technology, Faculty of Civil Engineering and Architecture, Chair of Historic Buildings Preservation,
656   *Budownictwo i Architektura*, **2010**, Vol. 7, pp. 131-144.
657 18. Adler, A.; Lionheart, W. RB. Uses and abuses of EIDORS: an extensible software base for EIT. *Physiological*
658   *measurement*, **2006**, 27.5: S25.
659 19. De Donno, G.; Di Giambattista L.; Orlando, L. High-resolution investigation of masonry samples through
660   GPR and electrical resistivity tomography. *Construction and Building Materials*, vol. 154, **2017**, p. 1234-1249.
661 20. Filipowicz, S.F.; Rymarczyk, T. Measurement Methods and Image Reconstruction in Electrical Impedance
662   Tomography, *Przeglad Elektrotechniczny*, **2012**, 88(6) 247-250
663 21. Rymarczyk T. New Methods to Determine Moisture Areas by Electrical Impedance Tomography,
664   *International Journal of Applied Electromagnetics and Mechanics*, **2016**, 52 79-87.
665 22. Sikora, J.; Wójtowicz, S. Industrial and Biological Tomography: Theoretical Basis and Applications, **2010**,
666   *IEL Warsaw*
667 23. Holder, D.S. Introduction to biomedical electrical impedance tomography Electrical Impedance
668   Tomography Methods, *History and Applications Bristol: Institute of Physics* **2005**
669 24. Karhunen, K.; Seppänen, A.; Lehikoinen, A., Monteiro; P.J.M., Kaipio J. P. Electrical Resistance
670   Tomography Imaging of Concrete. *Cement and Concrete Research*, **2010**, 40 137-145

671   25. Kłosowski, G.; Rymarczyk, T. Using neural networks and deep learning algorithms in electrical impedance
672   tomography. In *IAPGOS*, 3/**2017**, 99–102.
673   26. Wang M. Industrial Tomography: Systems and Applications, Elsevier, **2015**.
674   27. Efron, B.; Hastie, T.; Johnstone, I.; Tibshirani, R. Least Angle Regression, *The Annales of Statistics*, **2004**, vol.
675   32, No. 2, pp. 407-409.
676   28. Hastie, T.; Tibshirani, R.; Friedman, J. The Elements of Statistical Learning Data Mining, Inference, and
677   Prediction, Springer, New York, **2009**.
678   29. Karhunen, K.; Seppänen, A.; Kaipio, J. P. Adaptive meshing approach to identification of cracks with
679   electrical impedance tomography. *Inverse Problems & Imaging*, **2014**, 8(1) 127-148. doi: 10.3934/ipi.2014.8.127
680   30. Wehrens, R., Mevik, B.H.: The pls package: Principal Component and Partial Least Square Regressian in R.
681   *Journal of Statistical Software*, **2007**,   Vol. 18, nr 2.
682   31. Lechleiter, A.; Rieder, A. Newton regularizations for impedance tomography: convergence by local
683   injectivity. *Inverse Problems*, **2008**, 24(6) 065009
684   32. James, G.; Witten, D.; Hastie, T.; Tibshirani, R. *An Introduction to Statistical Learning with Applications in R*,
685   Springer, New York, **2013**.
686   33. Tibshirani, R. Regression shrinkage and selection via the lasso, Journal of the Royal Statistical Society,
687   Series B, **1996**, Vol. 58, nr. 1, pp. 267–288.
688   34. Demidenko, E.; Hartov, A.; Paulsen, K. Statistical estimation of Resistance/Conductance by electrical
689   impedance tomography measurements, *IEEE Transaction on Medical Imaging*, **2004**, Vol. 23, nr 7, pp.829-838.
690   35. Friedman, J.; Tibshirani, R.; Hastie, T. Regularization paths for generalized linear models via coordinate
691   descent, *Journal of Statistical Software*, **2010**, Vol. 33, nr 1.
692   36. Wehrens, R. Chemometrics with R. Multivariate Data Analysis in the Natural Science and Life Sciences,
693   Springer **2011**.
694   37. Zou, H., Hastie, T. Regularization and variable selection via the elastic net. *Journal of the Royal Statistical
695   Society*, Series B, **2005**, Vol. 67, nr 2, pp. 301–320.
696   38. Vincent, P.; Larochelle, H.; Lajoie, I.; Bengio, Y.; Manzagol, P. A. Stacked denoising autoencoders: Learning
697   useful representations in a deep network with a local denoising criterion. *Journal of Machine Learning
698   Research*, **2010**, *11*(Dec), 3371-3408.